



Multiscale interplay of curvature and hydrodynamic slippage in flow over a patterned topography

Mainendra Kumar Dewangan ^{1,*} and Subhra Datta ^{2,†}

¹*Department of Mechanical Engineering, Indian Institute of Technology Gandhinagar Palaji, Gujarat 382355, India*

²*Department of Mechanical Engineering, Indian Institute of Technology Delhi Hauz Khas, New Delhi 110016, India*



(Received 11 July 2021; accepted 2 February 2022; published 24 February 2022)

Reduction of fluid-solid friction utilizing the phenomenon of hydrodynamic slippage underlies a variety of energy-saving innovations. For simple demonstration of such ideas, the flow is often assumed to take place over a planar substrate. On the other hand, both roughness and intentionally textured topographies are ubiquitous in nature and engineering. Accordingly, a shear flow intrinsically slipping over a topography with small-amplitude corrugations is considered. Deriving scaling insights from a kinematic interpretation of the boundary conditions, a singular perturbation theory is developed for the multiscale interplay of the degree of intrinsic slip with the curvature of the surface along the slip velocity. Four distinct scaling regimes are identified. Especially for strongly (but not necessarily perfectly) slipping sinusoidal surfaces, unique analytical predictions with a wide intrinsic slip and amplitude range of numerical accuracy vis-à-vis finite element simulations are obtained, whereas the predictions on the small-slip scaling regimes corroborate findings from the literature. If the corrugation amplitude increases beyond a critical value, then strongly slipping surfaces suffer a slip-to-stick transition losing their lubricating properties. Unlike existing analytical predictions, the developed large-slip model can represent the slip-to-stick transition with reasonable accuracy, despite their rather simple analytical form. For extra accuracy, the predictions are readily extensible through computer algebra.

DOI: [10.1103/PhysRevFluids.7.024002](https://doi.org/10.1103/PhysRevFluids.7.024002)

I. INTRODUCTION

Hydrodynamic slip corresponds to a violation of the classical no-slip boundary condition for fluid solid interfaces [1] which leads to reduced friction. Slip of liquids at fluid-solid interfaces can significantly improve energy conversion efficiencies in applications such as desalination, pumping, and osmotic and electrokinetic power [2,3]. For fast transport of water, the multifunctional superhydrophobic surfaces and liquid infused surfaces [4] and nanomaterials such as graphene sheets and carbon nanotubes [5–7] show promising amplification of hydrodynamic slip. Except for unrealistically large shear rates, the linear Navier slip boundary condition is used to represent hydrodynamic slip [8].

While surface topographies feature prominently in many application areas such as microfluidics and nanotechnology [9–11], turbulent drag reduction [12–14], and geophysical flows [15], previous work has either inadequately or incorrectly explored the impact of hydrodynamic slippage on flow over topographies. In this study, we attempt to bring out the important role of local surface curvature

*mainendra1987@gmail.com

†subhra.datta@iitd.ac.in

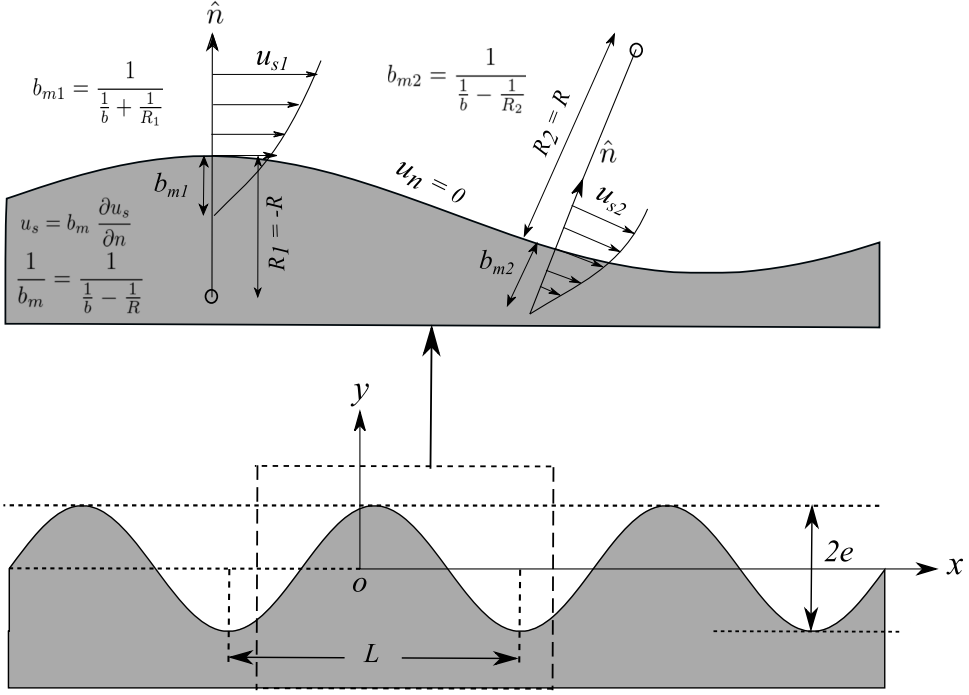


FIG. 1. Figure file updated with corrected aspect ratios. The geometry and coordinate system for analyzing shear-driven flow in the x - y plane over a sinusoidal surface pattern with amplitude e and wavelength L is shown on the lower panel. The upper panel is an inset of the lower panel showing the sign convention in and geometrical interpretation for the slip boundary condition for curved surface given by Eq. (1).

in the direction of the flow through a multiscale analysis and place particular theoretical focus on the less visited case of mildly sheared surfaces. This case is also technologically important due to the concomitant energy savings [6].

The Navier slip boundary condition for a Newtonian fluid of viscosity μ is often understood to imply a proportionality between the tangential flow speed u_s on the wall and the normal derivative of the tangential speed ($\frac{\partial u_s}{\partial n}$). Here n is a coordinate along the surface normal and s denotes a coordinate tangential to the wall velocity direction. As first derived in Ref. [16], for a general impervious curved surface in Newtonian fluid flow, while this proportionality is correct, the constant of proportionality is not the (intrinsic) “slip length” (b), as in planar surfaces. Unlike b , which can be perceived as a surface-geometry-independent intrinsic physicochemical property of the solid-liquid combination, the correct constant of proportionality, termed “mesoscopic slip length” (b_m) by Einzel *et al.* [16], is not “transferable” to other flow configurations [16–18]. The reason for the “nontransferability” is the dependence of b_m on the local curvature radius R of the surface along the wall slip velocity. As derived in Ref. [16], the mesoscopic slip length is given by

$$u_s = b_m \frac{\partial u_s}{\partial n}, \quad \text{where} \quad b_m = \frac{1}{\frac{1}{b} - \frac{1}{R}}. \quad (1)$$

Equivalently, $1/R$ is the normal curvature along the direction of the wall slip velocity. This boundary condition is depicted on the top panel of Fig. 1 along with the corresponding sign convention, *viz.* R is positive if the center of curvature of the osculating circle of the wall streamline lies in the liquid.

It can be noted that Eq. (1) is essentially a special case for Newtonian fluids of a boundary condition using the local tangential shear stress τ_{ns} , which can be expressed as

$$u_s = \frac{b}{\mu} \tau_{ns}. \quad (2)$$

This form of the Navier slip boundary condition is justifiable from coordinate invariance and equilibrium statistical-mechanics considerations [17,19]. Although less illuminating geometrically, this form is somewhat more general, as it is not mathematically restricted to fluid-impervious surfaces and a Newtonian viscosity law and is indeed the starting point for the derivation of Eq. (1) given in Ref. [16]. This form is also more straightforward to represent analytically and numerically. A kinematic interpretation of the wall shear strain rate component τ_{ns}/μ which is applicable to curved surfaces that are not necessarily an interface between two phases can be brought out using tools from differential geometry [20].

Correct statement and usage of Eq. (1) in its form for simple surface shapes such as sphere and cylinder and formulations involving direct use of Eq. (2) are recorded [17,21–24] both in the literature that predate and follow Ref. [16]. Reference [25] is also a follow-up study by the authors of Ref. [16] regarding the frictional resistance of periodic surface topographies [25]. Yet there are multiple studies, even in the recent literature [26–30], which confound between b_m and b , signifying the absence of the curvature effect in their models. Even Ref. [31], which laid the foundations of slip length measurement through atomic force microscopy and surface force apparatus [32,33], neglects curvature effects on effective slip.

The concept of effective slip length (b_{eff}) [12,34,35] consolidates from a solution of the flow field a single parameter to characterize the frictional resistance of the topographic features. The effective slip length (b_{eff}) can be interpreted as the distance below the mean topography height at which the feature-averaged streamwise velocity extrapolates to zero. Later in the study (Sec. II), a more precise definition is provided.

In the current work, the effective slip of periodic topographies with intrinsic slippage are investigated through local specification of the correct curvature-sensitive mesoscopic slip length. Accordingly, selected contributions on the effective slip of intrinsically slipping surfaces from the existing literature are examined more critically in the following paragraphs.

Reference [23] developed an asymptotic theory for Stokes flow over a sinusoidally wavy surface based on the assumption of the amplitude to wavelength ratio being small. Reference [36] shows that intrinsic slip and patterning effects additively superpose into the effective slip length in the “weak slip” limit, where in addition the ratio of the intrinsic slip length to amplitude is small.

The less-well-understood “mildly sheared surface” forms the opposite limit of the weakly slipping surface. The perfect slip or zero shear problem was studied theoretically in Ref. [37] and has gained more recent attention [38,39] in the context of understanding the limits of drag reduction by superhydrophobic surfaces. Superhydrophobic surfaces have topography-adherent vapor films of nonuniform shape termed “bubble mattresses,” for which theoretical treatment through the imposition of perfect slip or zero shear is an idealization of the best-case scenario [35,37,40,41]. However, a more realistic treatment should ascribe a finite but large local slip length to the nonplanar surface of the adherent vapor film, which makes such a surface “mildly sheared.” Effective slip when the intrinsic slip length is large but finite will be of particular interest to the current work. The methodological focus will also to maintain the analytical tractability of the intrinsic-slip dependence of the effective slip length, which only a few works have addressed so far for shear flows [23,25].

Analytical results on shear flow over a surface with large but not infinite degree of slippage are available only from Ref. [25], where the scaling characteristic of the zero shear limit is captured. Curiously, their results on effective slip (reproduced here in Appendix A) suggest that the zero shear effective slip and the intrinsic slip are inverse additive up to asymptotic order 8 in their amplitude to pattern wave-number product.

The theoretical considerations including scaling considerations and regimes and the spectral-asymptotic methodology used for modeling the effective slip of intrinsically slipping topographies

the current work is discussed in Sec. II. In particular, in Sec. II B, a systematic singular perturbation theory having four scaling regimes differing in the relative significance of curvature, normal velocity, and slippage effects is formulated in Sec. II B. In Sec. III, fully resolved Stokes-flow finite-element simulations are used to understand the utility and limitations of the current predictions and those from the literature.

II. THEORETICAL MODEL

Steady incompressible, shear-driven flow of a Newtonian fluid of viscosity μ over a corrugated surface is considered, as illustrated in Fig. 1. To get simple, specific, and numerically verifiable asymptotic representations of the effective slip length, the surface $y = e \cos \frac{2\pi x}{L}$ is considered. Here L is the wavelength and e is the amplitude of the corrugation. However, it is crucial to note here that the scaling laws and slip regimes discussed in Sec. II B apply to any periodic and smooth surface shape. Far from the surface ($y \rightarrow \infty$), the shear rate γ is specified. The shear flow model is appropriate for representing the near-wall pressure-driven flow in situations where corrugated or rough surfaces form the wall of a channel of finite characteristic size h , provided the ratio h/L is large [34]. Viscous diffusion on the scale of pattern wavelength is assumed to dominate advection, which would allow the Reynolds number to be set to zero in the governing equations. This simplifies the analysis and might be realistic for application areas such as microfluidics, nanotechnology, biology, and (even turbulent) drag reduction [9,12,13,42,43]. On the impermeable wall, the no-penetration criterion and the slip boundary condition [Eq. (2) or Eq. (1)] applies.

By choosing $\frac{L}{2\pi}$ as distance units in the x , y , and z directions, the dimensionless independent variables X , Y , and Z are introduced. The slip length is rendered dimensionless by defining $B = \frac{2\pi b}{L}$. The dimensionless amplitude is given by $\epsilon = \frac{2\pi e}{L}$ and will be treated as a small parameter in the subsequent asymptotic analysis.

In the following, our interest lies in the prediction of the dimensionless effective slip length obtained from its dimensional counterpart b_{eff} through $B_{\text{eff}} = \frac{2\pi b_{\text{eff}}}{L}$. The effective slip length characterizes the frictional resistance of the surface to the flow over it and can be calculated from the streamwise velocity U using [36]

$$B_{\text{eff},X} = \langle U \rangle_{Y=0}, \quad (3)$$

where the angular brackets denote averaging over one period of the pattern. As experimental geometries are wall bounded, there exists also an alternate paradigm of estimating the effective slip length from flow-rate predictions/measurements [1,44]; the B_{eff} above then is the limiting form for large channel height to pattern wavelength ratios [43].

Section II A begins the analysis with a spectral-asymptotic approach based on small ϵ . Novel scaling strategies based on the singular nature of the problem are introduced in Sec. II B, where the different distinguished limits and the corresponding scaling regimes are analyzed in detail.

A. Asymptotic solution

To obtain the flow field, a stream function $u = \Psi_Y$ and $v = -\Psi_X$ may be introduced, with subscripts indicating differentiation. The stream function satisfies $\nabla^4 \Psi = 0$, where ∇^2 is the Laplacian operator in the X - Y plane.

Equation (2) is considered as the slip boundary condition on the corrugated wall. Expressing the Cartesian form of the viscous stress tensor in the rotated local (tangent-normal or s – n) coordinate system at a point on the surface $y = \epsilon \cos(x)$ the dimensionless form of τ_{ns} , Equation (2) can be recast to

$$\Psi_Y + \epsilon \sin X \Psi_X = Bp[1 - \epsilon^2 \sin^2(X)][(\Psi_{YY} - \Psi_{XX}) + 4\epsilon \sin(X)\Psi_{XY}]. \quad (4)$$

where $p = [1 + \epsilon^2 \sin^2(X)]^{-1/2}$. The no-penetration condition can be enforced by setting the stream function on the corrugated wall to be zero. The far-field boundary conditions are $\Psi_{YY}(X, \infty) = 0$ and $\Psi_Y(X, \infty) = 1$.

The governing equation $\nabla^4 \Psi = 0$ for Stokes flow, periodicity, the far-field boundary conditions and Eq. (3) require Ψ to have the following general form:

$$\Psi(X, Y) = \frac{Y^2}{2} + B_{\text{eff}}Y + C_0 + \sum_{n=1}^{\infty} (C_{n1}e^{-nY} + C_{n2}Ye^{-nY}) \cos(nX). \quad (5)$$

To obtain the effective slip length B_{eff} and the associated constants C_0 and C_{n1} , an asymptotic-spectral procedure similar to that conducted in Ref. [18] is adopted. The left-hand side of Eqs. (4) and the no-penetration condition $\Psi(x, \epsilon \cos(x)) = 0$ are expanded in Taylor series, and the resultant expression is organized into a Fourier series through trigonometric simplifications. Finally, the coefficients of each Fourier mode up to a desired order (four to six harmonics for the reported results) is set to zero and the resultant truncation of the corresponding infinite linear equation system is solved algebraically. This process is conducted through symbolic computations in the software Mathematica from Wolfram Research.

In the above process, to explore multiple regimes of slippage topography interactions, we allow B to be ϵ dependent in a power-law form. Scaling arguments advanced in Sec. II B will help us understand the correct scaling to be adopted for each regime of interest.

B. Multiscale hydrodynamic slippage

In the current section, for varying degrees of slippage, a systematic singular perturbation theory having four “decks” (or scaling regimes) differing in the relative significance of curvature, normal velocity gradient, and slippage effects will be formulated. The effective slip length will be predicted. The focus will be on not having a large number of terms in the asymptotic expansion but on leveraging the right scales to get reasonably simple expressions that are likely to be accurate over an useful amplitude range.

1. Insights from the zero shear stress surface

The zero shear stress surface is desirable from the technological viewpoint of friction reduction and can be achieved, in principle, by allowing fluid to flow over a gas film completely coating a surface [41]. The nonzero X component of the surface traction force leads to a finite resistance of a curved surface to far-field flow in the X direction.

The no-penetration boundary condition demands

$$\epsilon \sin XU + V = 0 \text{ on } Y = \epsilon \cos(X). \quad (6)$$

For both terms to be important in Eq. (6), ϵU and V must be of the same asymptotic order. Also, the zero shear stress planar ($\epsilon = 0$) surface has no bounded solution, suggesting that both U and V should diverge in the small- ϵ limit. The weakest divergence for V admissible by a power series in integral powers of ϵ is $V = O(1/\epsilon)$. Consequently, it follows from Eq. (6) that $U = O(1/\epsilon^2)$. This finding based on a simple scaling argument will be verifiable against detailed calculations in Sec. II B 2 for finite hydrodynamic slip.

The no-shear boundary condition can be given the kinematic form $\frac{\partial U}{\partial n} + \frac{U}{R} = 0$, which is $b \rightarrow \infty$ limit of Eq. (1). For small ϵ , R is $O(1/\epsilon)$. So it follows that $\frac{\partial U}{\partial n} \sim \frac{\partial U}{\partial y} = O(1/\epsilon)$ as ϵ approaches zero.

The discussion in Sec. II B 2, where we study the interplay of curvature $1/R$ with partial intrinsic slip B and explore the large B limit will further corroborate these scaling laws. It can be also be noted here that the generalization of the above scaling laws to a more general smooth surface of the shape $Y = \epsilon g(X)$ merely involves replacing all instances of $\cos(X)$ by $g(X)$ and $\sin(X)$ by $-g'(X)$ in the equations of the current subsection.

TABLE I. Understanding curvature effects in transverse flow through the asymptotic behavior of terms in the kinematic form of slip boundary condition [Eq. (8)] and the no-penetration boundary condition [Eq. (7a)]. Here the “big O ” order symbol is used in the sense of “of order exactly.” The letter T is a shorthand for “Term” in Eq. (8).

B, U , and ϵV	$\frac{\partial U}{\partial n}$	Term 1 (T_1)	Term 2 (T_2)	Term 3 (T_3)	Dominant balance in Eq. (8)	Role of curvature
$O(\epsilon)$	$O(1)$	$O(1)$	$O(1)$	$O(\epsilon^2)$	$T_1 \sim T_2$	Insignificant
$O(1)$	$O(1)$	$O(1)$	$O(1)$	$O(\epsilon)$	$T_1 \sim T_2$	Slight
$O(\frac{1}{\epsilon})$	$O(1)$	$O(1)$	$O(1)$	$O(1)$	$T_1 \sim T_2 \sim T_3$	Important
$O(\frac{1}{\epsilon^2})$	$O(\frac{1}{\epsilon})$	$O(1)$	$O(\frac{1}{\epsilon})$	$O(\frac{1}{\epsilon})$	$T_2 \sim T_3$	Predominant

Interestingly, for a different surface corrugation shape (parametrically specified as $X = \alpha \frac{\sin(u)}{\pi} - \frac{u}{\pi}, Y = \frac{\alpha \cos(u)}{\pi}$), Ref. [37] finds through simplification of relations derived through conformal mapping [mentioned in Eq. (6.11) of this work] that the effective slip length $B_{\text{eff},X} = \langle U \rangle$ has a similar $O(1/\alpha^2)$ growth to infinity when the surface shape parameter α analogous to ϵ for the sinusoidal surface becomes small. Section II B 2 will now bring out certain important characteristics of the effective slip behavior.

2. Scaling laws, dominant balances, and effective slip

For the effect of slip to be significant, we start with the expectation that U is exactly of the order of B . Also, as ϵ is reduced, the streamwise perturbations in U must decay faster than those in a direction perpendicular to the surface. The resulting dominant balance implies $\frac{d^2 U}{dy^2} \sim 0$ in the semi-infinite domain and $B \frac{dU}{dy} \sim U$ on the boundary.

In the no-penetration condition and the kinematic form of the slip boundary condition, we want at least two terms contribute to the dominant balance. To distinguish slip from no slip, we always want a contribution from the derivative term in the slip boundary condition when considering the dominant balance. As summarized through Eq. (7), these considerations lead to the following observations on the order of the growth/decay rates:

$$\epsilon \sin XU + \underbrace{V}_{o(U)} = 0 \text{ on } Y = \epsilon \cos(X), \quad (7a)$$

and

$$\underbrace{U}_{\text{exactly } O(B)} = B \left(\underbrace{\frac{\partial U}{\partial n}}_{\text{exactly } O(1) \text{ or larger}} + \underbrace{\kappa}_{\text{exactly } O(\epsilon)} U \right) \text{ on } Y = \epsilon \cos(x). \quad (7b)$$

Here the description “exactly $O(1)$ ” should be taken to mean “ $O(1)$ but not $o(1)$ ” [45]; a precise but less familiar notation conveying the same idea is the “ord(1)” from Ref. [46].

Considering the asymptotic behavior of the three terms of Eq. (7b):

$$\underbrace{\frac{U}{B}}_{\text{Term 1}} - \underbrace{\frac{\partial U}{\partial n}}_{\text{Term 2}} - \underbrace{\kappa U}_{\text{Term 3}} = 0 \text{ on } Y = \epsilon \cos(x), \quad (8)$$

where the underbraces will assist in the scaling analysis of Table I.

Table I summarizes four possible distinguished limits in Eq. (8). Of these, the current work will pay special attention to the moderate and large slip cases with $B = O(1)$ and $B = O(\frac{1}{\epsilon^2})$ corresponding to the second and fourth rows. Incidentally, the predictions in Ref. [36] and Ref. [23] can be interpreted as “small B ” [$B = O(\epsilon^2)$] and moderate-to-small B [$B = O(\epsilon)$] theories, respectively.

TABLE II. Effective slip length calculated on the basis of different scaling laws between B and ϵ . Here B_i with $i = 1, 2, 3, 4$ are $O(1)$ quantities defined by the scaling formulas in the first column.

Scaled B	Effective slip length [$B_{\text{eff},X} + o(\epsilon^2)$] in terms of B_i	Effective slip length in terms of B
$B = B_1\epsilon$	$\epsilon B_1 - \epsilon^2$	$B - \epsilon^2$
$B = B_2$	$\frac{(-8B_2^3 - 18B_2^2 - 7B_2 - 4)\epsilon^2}{4(2B_2 + 1)} + B_2$	$B - \frac{(8B^3 + 18B^2 + 7B + 4)\epsilon^2}{8B + 4}$
$B = \frac{B_3}{\epsilon}$	$(\frac{23B_3^2}{8} - B_3^4)\epsilon^2 + (B_3^3 - \frac{7B_3}{4})\epsilon - B_3^2 + \frac{B_3}{\epsilon}$	$-B^4\epsilon^6 + \frac{1}{8}B^2(8B + 23)\epsilon^4 - \frac{1}{4}B(4B + 7)\epsilon^2 + B$
$B = \frac{B_4}{\epsilon^2}$	$-\frac{B_4(B_4^2 - 27B_4 - 109)\epsilon^2}{64(B_4 + 1)^3} + \frac{-5B_4^2 - 14B_4}{8(B_4 + 1)^2} + \frac{B_4}{\epsilon^2(B_4 + 1)}$	$\frac{B}{B\epsilon^2 + 1} + \frac{-5B^2\epsilon^4 - 14B\epsilon^2}{8(B\epsilon^2 + 1)^2} - \frac{B(B^2\epsilon^4 - 27B\epsilon^2 - 109)\epsilon^4}{64(B\epsilon^2 + 1)^3}$

Note that an independent clue for the scaling law to be used for large B corresponding to the last row of Table I can be obtained from the discussion of the zero shear stress surface in Sec. II B 1, where $\langle U \rangle = O(1/\epsilon^2)$ is argued from the scaling considerations.

The asymptotic procedure discussed in Sec. II A involved the scaling-aware specification of $B = B_i/\epsilon^{(i-2)}$ corresponding to the four distinguished limits outlined in the i^{th} data row of Table I. As in Sec. II B 1, the scaling regimes discussed in Table I are not limited to a specific surface shape, although the subsequent analysis will be for sinusoidal surfaces. The analytical expressions for effective slip length [up to $O(\epsilon^2)$ accuracy] obtained using various $B - \epsilon$ scaling laws accurate to $O(\epsilon^2)$ are shown in Table II.

In the next section, it would be shown through intercomparisons and cross-validation with full-scale numerical simulations how the developed theory fills the gaps left by the contributions from Refs. [16,23,25,36]. In particular, the situations of large to moderate degrees of intrinsic slippage will be given special attention.

III. RESULTS

While asymptotic predictions are meant to be applied when ϵ is sufficiently small, it is important also to know how big a numerical value of ϵ can such a prediction admit until it is no longer useful. Therefore, in this section the existing asymptotic predictions on effective slip will be evaluated against a complementary approach which places no restrictions on ϵ . Certain physical features of mildly sheared surfaces which can be counterintuitive, and which have bearing on the ϵ range of usefulness of the asymptotic theories will be brought out. Also, an improvement to the model of the previous section to handle a broad range of intrinsic slip magnitudes will be proposed.

The numerical validation of asymptotic theories involved finite-element simulation of the Stokes equations in the software COMSOL Multiphysics (COMSOL AB, Sweden). The numerical method was similarly to Ref. [18], except for the specification of Eq. (2) rather than the no-slip as boundary condition. An unstructured triangular mesh was used for discretization. The numerical simulation required fixing the vertical extent of the flow domain. In the results to be reported, size-of-domain and mesh-size effects were tested to be absent in the numerically predicted effective slip length up to four decimal places on both twofold grid-refinement and twofold domain enlargement.

If a surface is not flat, then even a zero shear curved surface has been demonstrated to resemble a no slip surface [37], as a consequence of the nonzero feature-average of the streamwise component of the local viscous traction τ_{nn} . A corrugated surface with intrinsic slippage can be termed sticky when the effective no-slip plane lies above the mean level of corrugations (as for a curved no-slip surface), else it is slippery. For large but finite values of B on a sinusoidal surface, Fig. 2 shows that a slip to stick transition occurs above $\epsilon \simeq 1$ as the numerically calculated B_{eff} changes sign. The transition is due to the progressive strengthening of the streamwise viscous force, as the surface becomes more uneven. As B is increased, the transition amplitude can be observed to become B insensitive, even though the B values of 3, 5, and 7 used in Fig. 2 are not nominally “large.” As shown in Fig. 2, numerical data can be represented accurately even in the stick zone ($\epsilon > 1$ approximately)

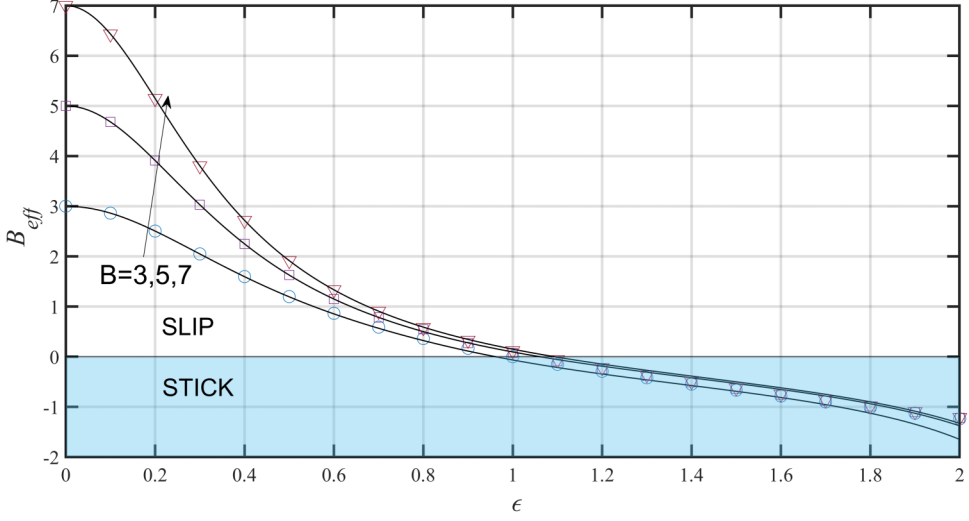


FIG. 2. Effective slip predictions from fully resolved simulations for $B = 3, 5, 7$ shown in symbols (circles, square, and triangle, respectively) compared against predictions from the range-extended large- B theory given by Eq. (B1) shown through solid lines.

through an analytical expression [Eq. (B1)]. Equation (B1) is a (4,4) Padé approximant with improved approximation characteristics [47] obtained through symbolic computation, although it may be argued that the corresponding analytical expression [Eq. (B1)] is somewhat cumbersome. It is desirable then to have simpler expressions, which as a compromise, accesses at least the large- B slip-stick transition amplitude ($\epsilon \simeq 1$) with a reasonable accuracy. No analytical theory available from the current literature can meet this requirement, as will be evident from the remainder of the current section, which will also redress the problem. However, it should be noted that if B is made progressively smaller, the start of the stick regime on the ϵ axis will eventually shift toward zero, in which case the theory Ref. [23] would become adequate up to the resultant transition amplitude.

The focus of the comparison, therefore, will be to understand the range of amplitudes over which the current model and the existing theories from the literature provide useful predictions. Particular attention will be given to the effective slip behavior of mildly sheared or strongly slipping surfaces. Series improvement through symbolic computations [18] to improve convergence at large amplitudes will be kept mostly out of scope in the spirit of avoiding long and cumbersome analytical expressions.

For convenience in numerical comparisons, we first reproduce from the last row and last column of Table II the most important large $-B$ result of the current study:

$$B_{\text{eff}} = \frac{B}{B\epsilon^2 + 1} - \frac{5B^2\epsilon^4 + 14B\epsilon^2}{8(B\epsilon^2 + 1)^2} - \frac{B(-109 - 27B\epsilon^2 + B^2\epsilon^4)\epsilon^4}{64(B\epsilon^2 + 1)^3}. \quad (9)$$

The finite limit of this expression, as $B \rightarrow \infty$, corresponds to the effective slip length of zero shear surface, whose scaling behavior was understood in Sec. II B 1. Further, if only the first term of Eq. (9) is retained as a leading-order approximation, then we get the expression $1/B_{\text{eff}} \simeq \frac{1}{1/B+1/\epsilon^2}$, which is able to corroborate the inverse additive property mentioned in Ref. [25]. However, Ref. [25] has claimed the validity of this handy approximation up to much larger asymptotic orders [Eq. (A5) is an $O(\epsilon^8)$ accurate approximation], which we are unable to corroborate. However, the predictions from Eqs. (A3)–(A5) will soon be shown to be inaccurate.

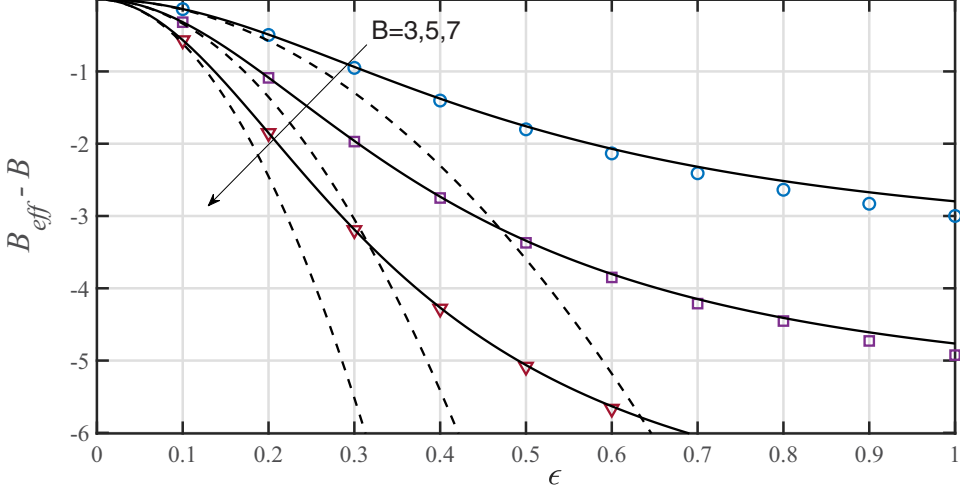


FIG. 3. Effective slip predictions from fully resolved simulations for $B = 3, 5, 7$ shown in symbols (circles, square, and triangle, respectively) compared against predictions from the large- B theory given by Eq. (9) shown through solid lines and the $O(\epsilon^2)$ accurate moderate- B theory of Ref. [23] given by Eq. (A1) and shown through dashed lines.

In the following discussion, Eq. (A1), which also occurs in the second row and last column of Table II, will be referenced extensively. This is an $O(\epsilon^2)$ accuracy moderate B prediction from Ref. [23].

Figure 3 suggests that for B values as small as $B = 3$, the formally “large- B ” [Eq. (9)] is accurate up to much larger ϵ values than the “moderate B ” [Eq. (A1)]. The range of ϵ over which a specified degree of accuracy is available from Eq. (9) expands significantly as B is increased to $B = 7$ through $B = 5$, while that from Eq. (9) shrinks significantly. The percentage error of the predictions at $\epsilon = 1$ was 6.75, 3.25, and 2% at $B = 3, 5$, and 7, respectively. However, as can also be reasonably expected, for small numerical values of B such as $B = 0.1$ (not shown here), Eq. (A1) was more accurate than Eq. (9).

The only other formally “large- B ” model for sinusoidal patterns available from the literature is that of Ref. [25]. As revealed by Fig. 4, compared to the current large- B model, the model in Ref. [25] is less accurate at any ϵ value, including the very small values ($\epsilon < 0.2$) shown on the inset.

Interestingly, the formal accuracy of the expressions in Ref. [25] as per the order symbols used by the author is $O(\epsilon^8)$, while Eq. (9) is formally $O(\epsilon^2)$ accurate. However, the deviation of predictions of Eq. (A3) from the numerical data is surprisingly nonmonotonic with zero crossings near $\epsilon \simeq 0.4$ and $\epsilon \simeq 0.9$. At $\epsilon = 0.2$, nearly 11.4% error is observed for Eq. (A3) compared to the modest 0.13% error by Eq. (9). In addition, the incorrect large-amplitude qualitative behavior of B_{eff} increasing with ϵ predicted by (A3) as seen on Fig. 4 is also of concern. Such mismatch with numerical data observed in Fig. 4 in terms of is suggestive of a possible analytical oversight in Ref. [25].

The singularity on the negative real ϵ^2 axis signified by the appearance of $B\epsilon^2 + 1$ in the denominator of each term of Eq. (9) confirms the zero-shear scaling law discussed in Sec. IIB 1 for $B \rightarrow \infty$. Interestingly, this form may be also responsible in part for this equation’s larger ϵ range of applicability relative to polynomial-form approximations such as Eq. (A1), which have inherent convergence limitations [49]. It can be noted here that series improvement approaches requiring a numerical estimate of the convergence radius [18,49] are not convenient here, while Padé approximants such as Eq. (B1) provide the convenience of analytically represent the intrinsic-slip dependence of effective slip.

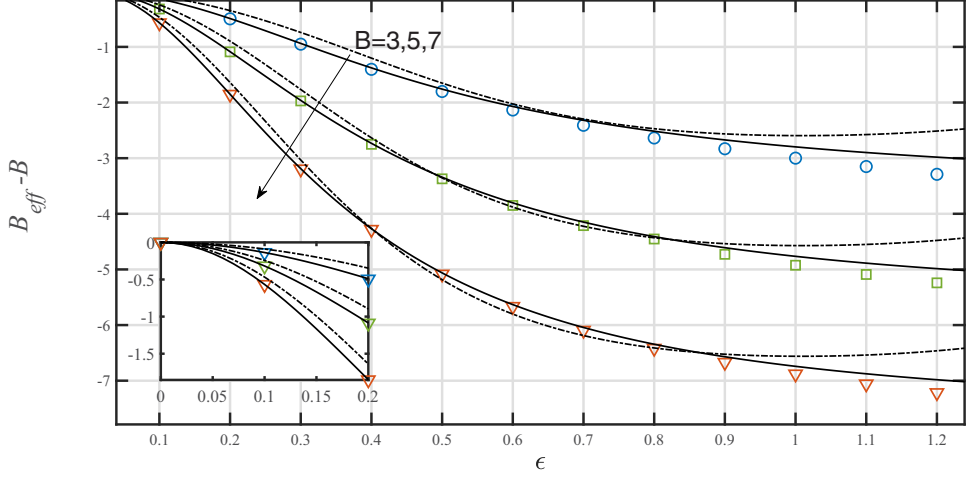


FIG. 4. Effective slip predictions from fully resolved simulations for $B = 3, 5, 7$ shown in symbols (circles, squares, and triangles, respectively) compared against predictions from the large- B theory given by Eq. (9) shown through solid lines and the large B theory from Ref. [25] given by Eq. (A3) and shown through dash-dotted lines.

Finally, we note that van Dyke’s matching principle [48] for obtaining composite asymptotic expansions can also be leveraged to obtain a single [$O(\epsilon^2)$ accurate] expression of the following form that can conveniently replace the two separate expressions in the second and fourth rows of Table II:

$$B_{\text{eff}} = -\frac{4B^2}{2B + \epsilon^2} + \frac{8B^2 - 4B + 7}{8B(B\epsilon^2 + 1)} + \frac{9(B - 2)}{8B(B\epsilon^2 + 1)^2} + \frac{81}{64B(B\epsilon^2 + 1)^3} + 2B + \frac{7}{64B} - \frac{53\epsilon^2}{64} - \frac{5}{8}. \quad (10)$$

In Fig. 5, numerical comparisons indicate that the composite expansion given by Eq. (10) more closely represents the numerical data for $B = 3$ and $B = 5$ than Eq. (9) at a given sufficiently small ϵ , as formally expected. In addition, the ϵ range of validity is also improved significantly, except for $B = 7$. The composite expansion was also found to have a larger range of accuracy at $B = 3, 5$, and 7 than the polynomial-form approximation for “moderately large” B appearing in the third row of Table I.

IV. CONCLUSIONS

The current work has derived new scaling laws and accurate closed-form models for fluid slipping past a corrugated wall. A systematic singular perturbation theory for small-amplitude corrugations having four scaling regimes [50] differing in the relative significance of curvature, normal velocity gradient and slippage effects has been formulated to obtain predictions for the effective slip length of sinusoidal corrugations. While the findings on the two large-slip regimes are unique contributions from the current study, the lower small-slip regimes corroborate findings from the literature [23,36]. The most important contribution of the study lies in its predictions for the regime with the largest slip which accurately represent surfaces that possess the largest (but still finite) intrinsic slip length.

Depending on the size of the corrugations, corrugated slipping surfaces may either be sticky (when the effective no-slip plane lies below the mean level of corrugations) or slippery. However

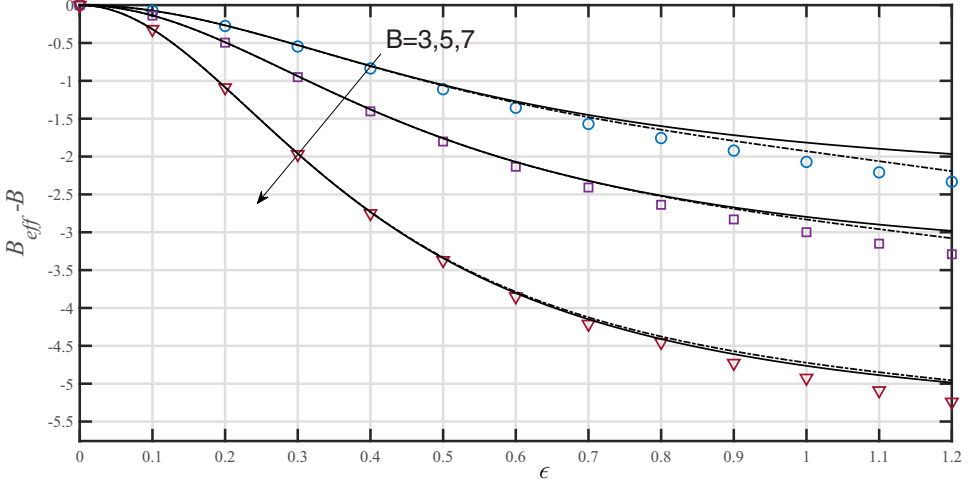


FIG. 5. Effective slip predictions from fully resolved simulations for $B = 3, 4, 5$ shown in symbols (circles, squares, and triangles, respectively) compared against predictions from the large- B theory given by Eq. (9) shown through solid lines and the composite expansion for moderate to large B given by Eq. (10) shown through dash-dotted lines.

large the degree of hydrodynamic slippage, sufficiently large groove sizes always lead to sticky behavior. The onset of sticky behavior is essentially due to the role of surface curvature. Given the rich interplay between curvature and slip observed here, it is surprising that the curvature of the wall streamline has been neglected in a large number of studies [26–30,36].

It emerges from the intercomparisons between our asymptotic and numerical analyses that despite a formal limitation to “small” values of the dimensionless amplitude, when a surface is mildly sheared, Eq. (9) can accurately access values of amplitude-wave-number product as large as unity for sinusoidal surfaces, which is improvement over predictions available from the literature. The developed large slip theory can also be made applicable to lower intrinsic slip values through the use of composite expansions derived through matched asymptotic analysis. While reasonably simple symbolic expressions are proposed for the intrinsic-slip and amplitude dependence of the effective slip, these findings are readily extendable through computer algebra if even larger amplitude-range of accuracy is needed [see, e.g., Eq. (B1)].

While the theoretical model leverages an elegant generalized representation of the local topography-slip interplay first derived in Ref. [16], the numerical comparisons also bring out the limitations of the only large-slip-limit effective slip prediction available in the literature from a companion study by the same authors [25]. Our analytical model also do not corroborate the inverse additive property of effective slip suggested in Ref. [25], except up to a certain asymptotic order [$O(\epsilon^2)$].

The findings of this work will be relevant to the development of low-friction superhydrophobic and lubricant-infused surfaces [51,52]. The findings may also complement the fundamental understanding of interfaces obtained through molecular simulations [53]. Non-planar topographies with large values of slip length also occur in exploratory experiments with novel hydrophobic materials (e.g., graphene and carbon nanotubes) that demonstrate the energy-saving property of superlubricity [53,54] to specific configurations of which the current findings might apply. Desalination, blue energy, and electrokinetic power are examples of applications where large hydrodynamic slippage is considered beneficial [3,55] and may yet get moderated by the surface topography.

ACKNOWLEDGMENTS

The authors acknowledge CSIR-HRDG for funding the research (Grant No. CSIR-HRDG-22(0854)/20/EMR-II).

APPENDIX A: ASYMPTOTIC PREDICTIONS FROM THE LITERATURE

In this section the key analytical results from Refs. [23,25] that would be used in the numerical comparisons to follow are summarized.

From Wang [23]: In the current notation, Eq. (34) of Wang [23] for transverse flow becomes

$$B_{\text{eff}} = B - \frac{(8B^3 + 18B^2 + 7B + 4)\epsilon^2}{4(2B + 1)} + O(\epsilon^4). \quad (\text{A1})$$

From Einzel *et al.* [25]: Equation (5.10) of Panzer [25] provides the following equations for transverse flow, valid for small and large values of intrinsic slip length B_0 , respectively:

$$B_{\text{eff}0} = B - \epsilon^2 \omega'_0(\epsilon) + \dots, \quad (\text{A2})$$

and

$$B_{\text{eff}\infty} = \left(\frac{1}{B} + \frac{\epsilon^2}{\omega'_\infty(\epsilon)} \right)^{-1} + \dots, \quad (\text{A3})$$

where

$$\omega'_0(\epsilon) = \frac{1 - \frac{1}{4}\epsilon^2 + \frac{19}{64}\epsilon^4 + O(\epsilon^6)}{1 + \epsilon^2 - \frac{1}{2}\epsilon^4 + O(\epsilon^6)} \quad (\text{A4})$$

and

$$\omega'_\infty(\epsilon) = \frac{1 - \frac{5}{4}\epsilon^2 + \frac{61}{64}\epsilon^4 + O(\epsilon^6)}{1 + \epsilon^2 - \frac{1}{2}\epsilon^4 + O(\epsilon^6)}. \quad (\text{A5})$$

APPENDIX B: HIGH ACCURACY PADÉ APPROXIMANT TO RESOLVE SLIP TO STICK TRANSFORMATION

With $B_4\epsilon^2 = B$, the eight-term power series for B_{eff} can be approximated using the (4,4) diagonal Padé approximant [18,48] for improving the amplitude range of validity through the following equation:

$$B_{\text{eff}} = \frac{\frac{(5807B_4^4 + 35798B_4^3 + 91398B_4^2 + 135936B_4 + 64512)\epsilon^4}{1152B_4(B_4+1)(B_4^2-27B_4-109)} + \frac{(-1255B_4^4 - 2593B_4^3 + 480B_4^2 - 12672B_4 - 4608)\epsilon^2}{144B_4(B_4+1)(B_4^2-27B_4-109)} + \frac{B_4}{B_4+1}}{\frac{(-1165B_4^5 - 6026B_4^4 - 18727B_4^3 - 39660B_4^2 - 17280B_4 - 4608)\epsilon^4}{144B_4^2(B_4+1)(B_4^2-27B_4-109)} + \epsilon^2}. \quad (\text{B1})$$

-
- [1] E. Lauga, M. Brenner, and H. A. Stone, Microfluidics: The no-slip boundary condition, in *Handbook of Experimental Fluid Mechanics*, edited by C. Tropea, A. Yarin, and J. F. Fouss (Springer, New York, 2007), chap. 19, pp. 1219–1240.
 - [2] M. Napoli, J. C. Eijkel, and S. Pennathur, Nanofluidic technology for biomolecule applications: A critical review, *Lab Chip* **10**, 957 (2010).
 - [3] A. Siria, M.-L. Bocquet, and L. Bocquet, New avenues for the large-scale harvesting of blue energy, *Nat. Rev. Chem.* **1**, 0091 (2017).
 - [4] S. Peppou-Chapman, J. K. Hong, A. Waterhouse, and C. Neto, Life and death of liquid-infused surfaces: A review on the choice, analysis and fate of the infused liquid layer, *Chem. Soc. Rev.* **49**, 3688 (2020).

- [5] M. Majumder, N. Chopra, R. Andrews, and B. Hinds, Nanoscale hydrodynamics: Enhanced flow in carbon nanotubes, *Nature (Lond.)* **438**, 44 (2005).
- [6] K. Falk, F. Sedlmeier, L. Joly, R. R. Netz, and L. Bocquet, Molecular origin of fast water transport in carbon nanotube membranes: Superlubricity versus curvature dependent friction, *Nano Lett.* **10**, 4067 (2010).
- [7] E. Secchi, S. Marbach, A. Niguès, D. Stein, A. Siria, and L. Bocquet, Massive radius-dependent flow slippage in carbon nanotubes, *Nature (Lond.)* **537**, 210 (2016).
- [8] P. A. Thompson and S. M. Troian, A general boundary condition for liquid flow at solid surfaces, *Nature (Lond.)* **389**, 360 (1997).
- [9] A. D. Stroock, S. K. Dertinger, A. Ajdari, I. Mezić, H. A. Stone, and G. M. Whitesides, Chaotic mixer for microchannels, *Science* **295**, 647 (2002).
- [10] P. Garg, J. Picardo, and S. Pushpavanam, Chaotic mixing in a planar, curved channel using periodic slip, *Phys. Fluids* **27**, 032004 (2015).
- [11] E. S. Asmolov, A. L. Dubov, T. V. Nizkaya, A. J. Kuehne, and O. I. Vinogradova, Principles of transverse flow fractionation of microparticles in superhydrophobic channels, *Lab Chip* **15**, 2835 (2015).
- [12] D. Bechert and M. Bartenwerfer, The viscous flow on surfaces with longitudinal ribs, *J. Fluid Mech.* **206**, 105 (1989).
- [13] P. Luchini, F. Manzo, and A. Pozzi, Resistance of a grooved surface to parallel flow and cross-flow, *J. Fluid Mech.* **228**, 87 (1991).
- [14] J. Chang, T. Jung, H. Choi, and J. Kim, Predictions of the effective slip length and drag reduction with a lubricated micro-groove surface in a turbulent channel flow, *J. Fluid Mech.* **874**, 797 (2019).
- [15] N. Lahaye and S. G. Llewellyn Smith, Modal analysis of internal wave propagation and scattering over large-amplitude topography, *J. Phys. Oceanogr.* **50**, 305 (2020).
- [16] D. Einzel, P. Panzer, and M. Liu, Boundary Condition for Fluid Flow: Curved or Rough Surfaces, *Phys. Rev. Lett.* **64**, 2269 (1990).
- [17] W. Chen, R. Zhang, and J. Koplik, Velocity slip on curved surfaces, *Phys. Rev. E* **89**, 023005 (2014).
- [18] M. K. Dewangan and S. Datta, Improved asymptotic predictions for the effective slip over a corrugated topography, *Appl. Math. Model.* **72**, 247 (2019).
- [19] L. Bocquet and E. Charlaix, Nanofluidics, from bulk to interfaces, *Chem. Soc. Rev.* **39**, 1073 (2010).
- [20] S. Datta and M. K. Dewangan, Strain rate on curved surfaces: A differential-geometric approach, *Mech. Res. Commun.* **110**, 103633 (2020).
- [21] A. B. Basset, *A Treatise on Hydrodynamics: With Numerous Examples*, Vol. 2 (Deighton, Bell and Company, Cambridge, UK, 1888).
- [22] C. Wang, Stokes slip flow through a grid of circular cylinders, *Phys. Fluids* **14**, 3358 (2002).
- [23] C. Wang, Shear flow over a wavy surface with partial slip, *J. Fluids Eng.* **132**, 084503 (2010).
- [24] R. Barber, Y. Sun, X. Gu, and D. Emerson, Isothermal slip flow over curved surfaces, *Vacuum* **76**, 73 (2004).
- [25] P. Panzer, M. Liu, and D. Einzel, The effects of boundary curvature on hydrodynamic fluid flow: Calculation of slip lengths, *Int. J. Mod. Phys. B* **6**, 3251 (1992).
- [26] N. J. Lund, X. P. Zhang, K. Mahelona, and S. C. Hendy, Calculation of effective slip on rough chemically heterogeneous surfaces using a homogenization approach, *Phys. Rev. E* **86**, 046303 (2012).
- [27] A. A. Hemeda and H. V. Tafreshi, Instantaneous slip length in superhydrophobic microchannels having grooves with curved or dissimilar walls, *Phys. Fluids (1994-present)* **27**, 102101 (2015).
- [28] W. K.-H. Chu, Stokes slip flow between corrugated walls, *Z. Angew. Math. Phys.* **47**, 591 (1996).
- [29] M. Vasudeviah and K. Balamurugan, Stokes slip flow in a corrugated pipe, *Int. J. Eng. Sci.* **37**, 1629 (1999).
- [30] M. Vasudeviah and K. Balamurugan, On forced convective heat transfer for a stokes flow in a wavy channel, *Int. Commun. Heat Mass Transfer* **28**, 289 (2001).
- [31] O. I. Vinogradova, Drainage of a thin liquid film confined between hydrophobic surfaces, *Langmuir* **11**, 2213 (1995).
- [32] R. Pit, H. Hervet, and L. Léger, Friction and slip of a simple liquid at a solid surface, *Tribol. Lett.* **7**, 147 (1999).

- [33] L. Zhu, P. Attard, and C. Neto, Reconciling slip measurements in symmetric and asymmetric systems, *Langmuir* **28**, 7768 (2012).
- [34] E. Tuck and A. Kouzoubov, A laminar roughness boundary condition, *J. Fluid Mech.* **300**, 59 (1995).
- [35] J. R. Philip, Flows satisfying mixed no-slip and no-shear conditions, *Z. Angew Math. Phys.* **23**, 353 (1972).
- [36] K. Kamrin, M. Z. Bazant, and H. A. Stone, Effective slip boundary conditions for arbitrary periodic surfaces: The surface mobility tensor, *J. Fluid Mech.* **658**, 409 (2010).
- [37] S. Richardson, On the no-slip boundary condition, *J. Fluid Mech.* **59**, 707 (1973).
- [38] M. Sbragaglia and A. Prosperetti, A note on the effective slip properties for microchannel flows with ultrahydrophobic surfaces, *Phys. Fluids* **19**, 043603 (2007).
- [39] D. G. Crowdy, Effective slip lengths for immobilized superhydrophobic surfaces, *J. Fluid Mech.* **825** (2017).
- [40] A. Steinberger, C. Cottin-Bizonne, K. P., and E. Charlaix, High friction on a bubble mattress, *Nat. Mater.* **6**, 665 (2007).
- [41] E. Karatay, A. S. Haase, C. W. Visser, C. Sun, D. Lohse, P. A. Tsai, and R. G. Lammertink, Control of slippage with tunable bubble mattresses, *Proc. Natl. Acad. Sci. USA* **110**, 8422 (2013).
- [42] R. Choudhary, T. Bhakat, R. K. Singh, A. Ghubade, S. Mandal, A. Ghosh, A. Rammohan, A. Sharma, and S. Bhattacharya, Bilayer staggered herringbone micro-mixers with symmetric and asymmetric geometries, *Microfluid. Nanofluid.* **10**, 271 (2011).
- [43] M. K. Dewangan and S. Datta, Effective permeability tensor of confined flows with wall grooves of arbitrary shape, *J. Fluid Mech.* **891**, A12 (2020).
- [44] A. D. Stroock, S. K. Dertinger, G. M. Whitesides, and A. Ajdari, Patterning flows using grooved surfaces, *Anal. Chem.* **74**, 5306 (2002).
- [45] D. E. Knuth, Big omicron and big omega and big theta, *ACM Sigact News* **8**, 18 (1976).
- [46] E. J. Hinch, *Perturbation Methods* (Cambridge University Press, Cambridge, UK, 1991).
- [47] M. Van Dyke, Slow variations in continuum mechanics, *Adv. Appl. Mech.* **25**, 1 (1987).
- [48] M. Van Dyke, *Perturbation Methods in Fluid Mechanics* (The Parabolic Press, Stanford, 1975).
- [49] M. Van Dyke, Analysis and improvement of perturbation series, *Q. J. Mech. Appl. Math.* **27**, 423 (1974).
- [50] R. Meyer, A view of the triple deck, *SIAM J. Appl. Math.* **43**, 639 (1983).
- [51] B. R. Solomon, X. Chen, L. Rapoport, A. Helal, G. H. McKinley, Y.-M. Chiang, and K. K. Varanasi, Enhancing the performance of viscous electrode-based flow batteries using lubricant-impregnated surfaces, *ACS Appl. Energy Mater.* **1**, 3614 (2018).
- [52] M. Sbragaglia, R. Benzi, L. Biferale, S. Succi, K. Sugiyama, and F. Toschi, Generalized lattice boltzmann method with multirange pseudopotential, *Phys. Rev. E* **75**, 026702 (2007).
- [53] L. Guo, S. Chen, and M. O. Robbins, Effective slip boundary conditions for sinusoidally corrugated surfaces, *Phys. Rev. Fluids* **1**, 074102 (2016).
- [54] X. Zhang, R. Manica, Y. Tang, P. Tchoukov, Q. Liu, and Z. Xu, Probing boundary conditions at hydrophobic solid–water interfaces by dynamic film drainage measurement, *Langmuir* **34**, 12025 (2018).
- [55] Y. Ren and D. Stein, Slip-enhanced electrokinetic energy conversion in nanofluidic channels, *Nanotechnology* **19**, 195707 (2008).